International Journal of Mechanical Sciences 161–162 (2019) 105017

Contents lists available at ScienceDirect

International Journal of Mechanical Sciences

journal homepage: www.elsevier.com/locate/ijmecsci

# Extended finite element analysis of plastic and fracture behaviors of SiC-based multi-layer thin films system

Jixi Deng, Ningbo Liao*, Miao Zhang, Wei Xue

*College of Mechanical & Electrical Engineering, Wenzhou University, Wenzhou 325035, PR China*

ARTICLE INFO

*Keywords:*
Silicon oxycarbide
Nano-indentation
Thin film
Extended finite element method
Fracture

ABSTRACT

The interfacial mechanics of silicon oxycarbide (SiCO) thin films is a key factor for its applications as low dielectric constant (low K) materials, and it is very challenging for current experimental technologies to investigate the interfacial fracture of the materials system. In this work, nano-indentation induced plastic behavior and fracture properties of SiCN/SiCO/SiCN low K system are evaluated and predicted by extended finite elements method. To improve the accuracy of the model, an interfacial layer is added at the SiCO/SiCN and SiCN/Si substrate interfaces of the system. Based on the improved model, the calculated load - displacement curves consist nicely with the experimental data in all the indentation stages, and the mechanical behavior relating to interfacial delamination is successfully captured. Moreover, the indentation-dependent of Young's modulus and hardness are predictied, and the plastic properties of the films are obtained by calculating stress-strain relationship. The crack propagation paths and the calculated energy release rates are comparable to the experimental results.

## 1. Introduction

In order to reduce the serious problems of resistance and capacitance delay in integrated circuit field, a large number of low dielectric constant (low K) materials have been developed into inter-metallic dielectric materials to replace the traditional dielectric material [1,2]. Dielectric materials generally present high tolerance to mechanical damage, while porous low-k films show relatively poor mechanical properties, making it difficult to be used in structures below 90 nm [3]. The mechanical damage of porous low k layer is seriously affected by chemical-mechanical polishing and thermal stress. In particular, interfacial failure can adversely influence the performance of integrated circuits and leads to more serious problems such as current leakage [4,5]. In order to evaluate the interfacial adhesion strength of thin films, several measuring technologies have been developed [6–8]. The interfacial adhesion strength can be determined by measuring the film lamination caused by accumulation of interfacial shear stress.

Nano-indentation is a commonly used method to analyze the elastic modulus and hardness of thin films and coatings [9–11]. However, it is very hard for nano-indentation to provide details of the local stress distribution, stress concentration and fracture behavior of the systems [10,12]. Furthermore, it costs significant time and it cannot be applied in some extreme conditions. Extended finite element method (XFEM) can be used to simulate fracture of nano-materials, and it can deal with complex problems that are difficult to be solved analytically [13–17]. The interfacial properties and fracture toughness can be obtained by inputting critical stress/energy as criteria for nucleation and propagation of cracks [18–20], and the fracture related mechanical properties can be determined [21–23]. XFEM was used to investigate the effect of nano-voids and nano-cracks on the mechanical properties of a host medium [24], the simulation results demonstrated that randomly oriented crack gave an effective modulus lying between those of horizontal and vertical cracks. A XFEM approach was proposed for fracture in nano-composite based on mesh independent fiber-matrix interface, where the level set and 12-asymptotic function were used for describing interface geometry and bi-material crack tip [25].

In order to investigate interfacial mechanics of SiC-based multi-layer low-k thin films system, in this work, a nano-indentation model composed of nano-indenter and SiC-based multi-layer thin films are established, and the plastic and fracture behaviors of the system are studied by using extended finite element method. By comparing the simulated loading depth (p-h) curve with the experimental results, the adhesion strength of the interface is obtained, and the delaminating behavior of the interface is predicted to evaluate the reliability of the multilayer interconnection structure.

## 2. Computational methods

The nano-indentation in SiCN/SiCO/SiCN/Si multilayered film stack structure was numerically simulated by extended finite element method

* Corresponding author.
*E-mail address:* lnb55@163.com (N. Liao).

https://doi.org/10.1016/j.ijmecsci.2019.105017
Received 27 March 2019; Received in revised form 2 July 2019; Accepted 9 July 2019
Available online 9 July 2019

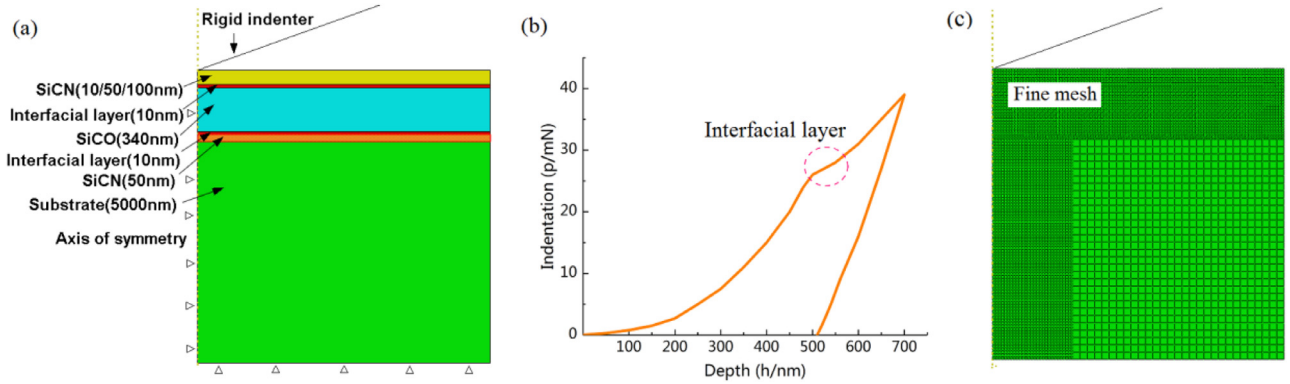


**Fig. 1.** (a) XFEM model for multi-layer system, (b) acquisition of interfacial layer and (c) mesh structure of the thin films system.

[21]. Two dimensional models were used in the nano-indentation simulation, as the differences of two dimensional and three dimensional models were less than 3% by our test simulation. Moreover, ideal conical hardness tester with pressure angle of 70.3° was applied in this work, which was also used in previous works [26,27]. Eight nodes and a bilinear axisymmetric simplified integral element (C3D8R) were used for the thin films, which were proved to present better performance on local stress concentration area of thin films under indenter. Four-node quadrilateral element (R3D4), quadrilateral element and simplified integral element were used for silicon substrate, as they showed better accuracy for small displacement without contact problem.

As shown in Fig. 1(a), the thicknesses of Si substrate, SiCO interlayer and bottom SiCN layer were 20 um, 340 nm and 50 nm respectively. In order to explore the influence of thickness on plastic and fracture properties, three models with thicknesses of 100 nm (model 1), 50 nm (model 2) and 10 nm (model 3) for top SiCN layer were established. Model 1 was established based on the multi-layer structure in experiment [28]. During the nano-indentation process, the shear stress accumulate at the interface between SiCO and SiCN layer due to the strain mismatch. With the load increases further, the interfacial fracture will induce stress release and deviation of the load - displacement curve.

To describe the mechanical properties of interfaces between Si, SiCN and SiCO, an interfacial layer with a thickness of 10 nm was added to each interface. The materials parameters of the interfacial layer were obtained from the small platform in load-displacement curve of the thin films system, as shown in Fig. 1(b), as the change in the slope of the curve corresponds to different material layer. The pressure head has only one degree of freedom downward and is in direct contact with the thin films. As a refined mesh would improve the accuracy of XFEM, uneven mesh segmentation was adopted and a denser mesh was used near the pressure head, as shown in Fig. 1(c).

Isotropic elastic-plastic behavior and Von Mises yield criterion for plastic flows were applied in calculations. The strain hardening exponent (n) was 0.1, which is applicable for most of the porous film material. At the indentation depth of 700 nm, the materials parameters of the thin films were measured through the nano-indentation experiment, as shown in Table 1.

To calculate fracture toughness of the films on silicon substrate, the maximum initial damage stress ($\sigma_{max}$) and the corresponding crack separation distance ($\delta_c$) were calculated firstly. The maximum initial damage stress ($\sigma_{max}$) at the start of cracking is the maximum principal stress in the depth of a fracture. As shown in Fig. 2, the maximum principal stress corresponding to different indentation depths are obtained through finite elements method. The indentation depths at the beginning of fracture are obtained as 140 nm, 220 nm and 290 nm. Thus, the maximum principal stresses at the beginning of fracture are calculated as 0.51 GPa, 0.59 GPa and 0.73 GPa. The crack separation distances are obtained as 5 nm, 5.5 nm and 5.3 nm by fitting the load displacement curves.

**Table 1**
Mechanical properties of thin films and substrate materials.

| | Young's modulus (E) GPa | Hardness GPa | Poisson's ratio ($\nu$) |
|---|---|---|---|
| Si substrate | 187 | 8.9 | 0.278 |
| SiCN | 95 | 7 | 0.31 |
| SiCO | 11 | 1.4 | 0.25 |

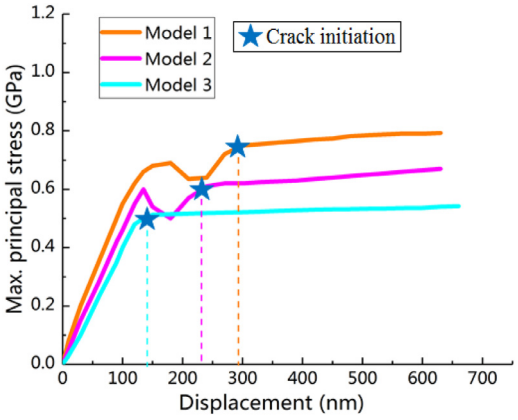


**Fig. 2.** The maximum principal stresses at different depths.

## 3. Results and discussions

The load - displacement (p-h) curves for the three models with and without interfacial layer are obtained and compared with those from experiments [28]. As shown in Fig. 3(a), the load - displacement curves of the models without interfacial layer can not reproduce the platform in experiments. By adding the interfacial layer, the resulting load - displacement curves of model 1 consist with experimental data in all the stages. The platform starts from the depth of 480 nm in experiment corpesonds to the interfacial delamination, and is repoduced by model 1 with interfacial layer. It means the presence of the transition layer successfully capture the mechanical behavior of interfaces, verifying the accuracy of the proposed approach. Moreover, with a decreasing thickness of SiCN layer, the indentation depths for interfacial delamination are predicted as 390 nm and 360 nm for model 2 and mode 3, respectively.

In order to better describe the plastic deformation behavior of materials, the power law function based on the power hardening model was used to characterize the stress-strain relationship of the silicon nitrogen coating [21,29,30]. Therefore, the stress-strain curve of the coating can be described as:

$$\sigma = \begin{cases} E\varepsilon, & \sigma < \sigma_y \\ K\varepsilon^n, & \sigma \geq \sigma_y \end{cases} \quad (1)$$

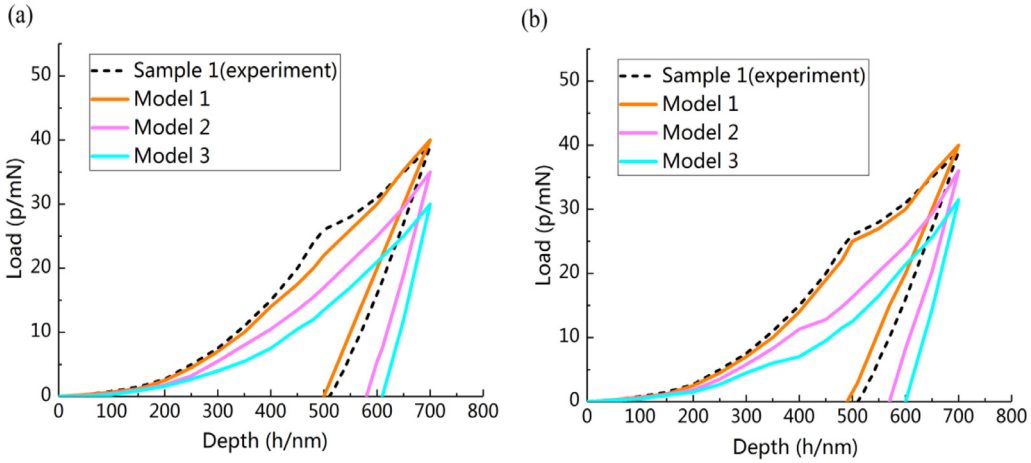


**Fig. 3.** The load - displacement curves for the three models (a) without and (b) with interfacial layer and are compared with those from experiments [28].

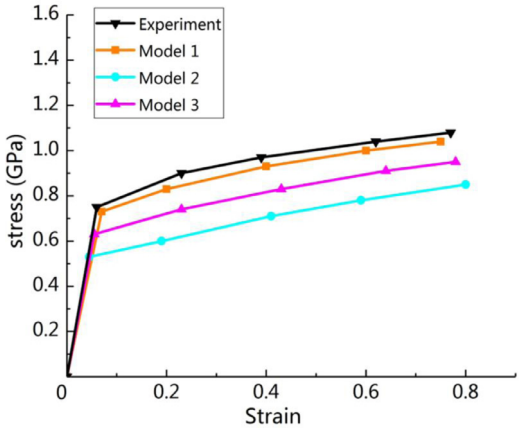


**Fig. 4.** Stress-strain relationships of the films obtained from XFEM simulations, and are compared with experimental results [28].

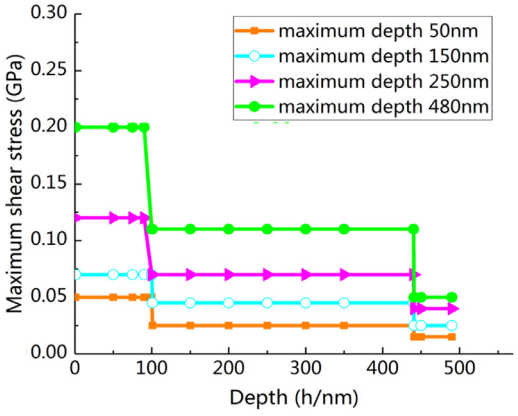


**Fig. 6.** The indentation depth dependent maximum shear stresses at different maximum depths.

where $E$, $\varepsilon$, $\sigma_y$ and n are Young's modulus, total strain, yield strength and strain hardening exponent, and K is strength coefficient. The strain hardening index is set as 0.1, which is applicable to the most of porous ceramics film. After several iterations and error analysis, the stress-strain behaviors of the thin films systems are predicted and compared with experimental results [28], as shown in Fig. 4.

Fig. 5(a)–(c) shows the stress distribution of model 1 with different indentation depths. At an indentation depth of 290 nm, the stress is concentrated near the indentation head, the maximum stress is 0.89 GPa and is greater than the maximum initial damage stress (0.73 GPa) of the thin films system, leading to the initialtion of a crack in the thin films. With theincreasing of indentation depth, the stress concentration shifts from the pressure head to the SiCO-SiCN interface, which is caused by the difference in mechanical properties of films. During the loading process, the matrix is highly compressed in the proximal region and accumulates at the indented edge. In particular, when the crack propagates to the interface, the local plastic accumulation around the contact area is strengthened and a large amount of accumulation occurs, and finally leads to interfacial delamination at indentation depth of 500 nm, which is consistent with the phenomenon observed in experiment [28].

Shear stress is a significant basis to judge interfacial bond strength. Fig. 6 shows the maximum shear stress along the direction perpendicular to the interface, with maximum indentation depth of 50 nm, 150 nm, 250 nm and 480 nm respectively. The results showed that shear stress varied greatly at the interfaces of SiCN (top)/SiCO (100 nm), SiCO/SiCN (bottom) (440 nm) and SiCN (bottom) /Si (490 nm).

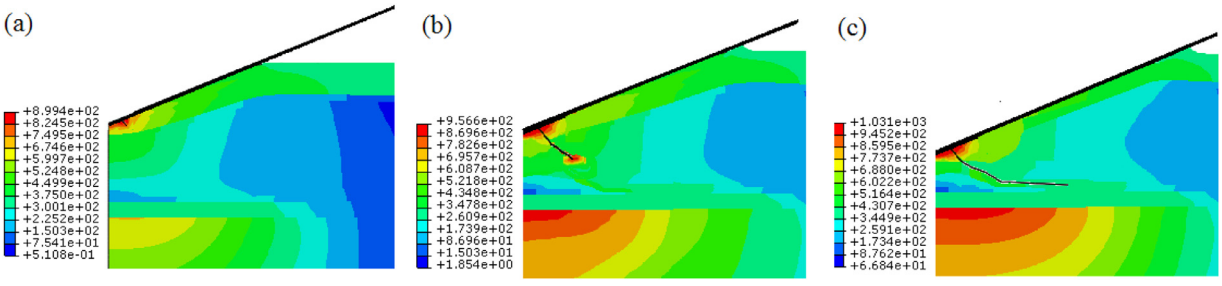


**Fig. 5.** The stress distribution of model 1 with indentation depths of 290 nm, 450 nm and 500 nm.

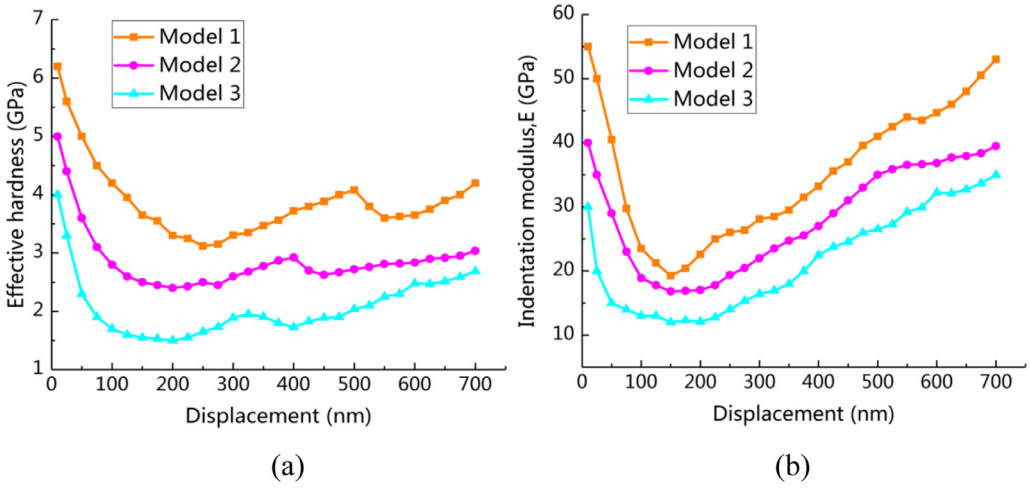


**Fig. 7.** The effective hardness (a) and Young's modulus (b) of the films system at different indentation depths.

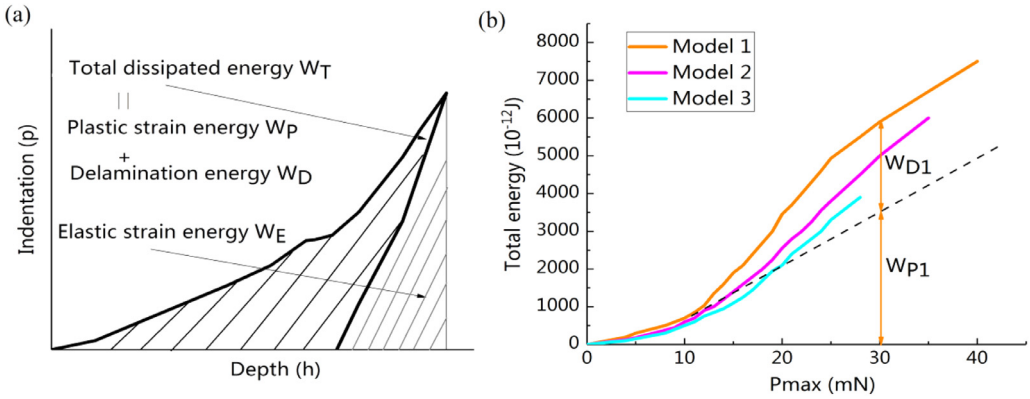


**Fig. 8.** The constitutions of total energy (a) and the calculated total energies at different maximum indentation load (b).

Fig. 7 shows the indentation depth dependent effective hardness and Young's modulus profiles of the films systems obtained from the nano-indentation simulation. In relatively low indentation depth (<100 nm), the effective hardness and Young's modulus decrease sharply with depth increases, corresponding to the properties transferring from top SiCN film to SiCO film. When the indentation depth is increased further, the hardness and Young's modulus gradually increase under the influence of bottom SiCN film. When the three models are at indentation depths of 300, 390 and 480 nm, their hardness show suddenly drop due to interface delaminating, and tend to increase again because of substrate effect. However, the interfacial failure cannot be inferred from the profile of Young's modulus, as the models show very subtle changes on Young's modulus during interfacial delamination.

The total energy of indentation load on thin film includes plastic strain energy, delamination energy and elastic strain energy, as shown in Fig. 8(a). Most of the elastic strain energy is released during unloading, while plastic energy is dissipated in the form of heat flow through plastic flow during the process of loading and unloading. When interface delamination happens during the loading process, the total dissipated energy $W_T$ is the sum of plastic dissipated energy $W_P$ and delamination dissipated energy $W_D$. By assuming the interfacial delamination develops from contact center of indentation and evolve into the triangular edges with circular geometry, the delamination area and energy release rate (G) can be determined [31].

Fig. 8(b) shows the relationship between the total dissipated energy $W_T$ and the maximum indentation load. With the increase of the maximum indentation load, the total dissipated energy increases obviously, which is consistent with the experimental conclusions. The slope of load-energy profile would change when SiCO/Si interface start to delaminate. The ratio of $W_P$ and $W_D$ is determined by the crossover point of linear part of the curve (as shown by the dashed line) and the vertical line at critical load. Thus, a critical load of 30 mN and a delamination dissipated energy of $5800 \times 10^{-12}$ J for model 1 corresponding to interfacial failure can be obtained. Thus, the energy release rate of model 1 is calculated as 1.73 $J \cdot m^{-2}$, which is comparable to the experimental value of $G = 1.68 J \cdot m^{-2}$ [28]. The energy release rate of model 2 and model 3 are predicted to be 1.46 $J \cdot m^{-2}$ and 1.24 $J \cdot m^{-2}$ respectively.

## 4. Conclusions

In this work, nano-indentation induced plastic and fracture behaviors of SiC-based multi-layer thin films are evaluated and predicted by simulating nano-indentation using extended finite elements method. To improve the accuracy of the model, an interfacial layer is added at SiCO/SiCN and SiCN/Si substrate interfaces in the system. The materials properties of the interfacial layer are obtained from nano-indentation test, the maximum initial damage stress and the corresponding crack separation distance of the films are evaluated from finite element simulation. Based on the improved model and inputting parameters, the calculated load - displacement curves consist nicely with the experimental data in all the indentation stages, and the mechanical behavior relating to interfacial delamination is successfully captured. The indentation-dependent of Young's modulus and hardness are predictied, and the plastic properties of the films are obtained by calculating stress-strain relationship. The crack propagation path is consistent with experimental conclusions, and the calculated energy release rates of model 1 is calcu-

lated as 1.73 $J \cdot m^{-2}$, which is comparable to the experimental value of $G = 1.68 J \cdot m^{-2}$.

## Acknowledgments

The authors would like to acknowledge the support of the National Natural Science Foundation of China (51675384).

## References

[1] Yuan C, Jin K, Li K, Diao S, Tong J, Fang Q. Non-porous low-k dielectric films based on a new structural amorphous fluoropolymer. Adv Mater 2013;25(35):4875–8.
[2] Nordell BJ, Nguyen TD, Caruso AN, Purohit SS, Oyler NA, Lanford WA, Gidley DW, Gaskins JT, Hopkins PE, Henry P. Carbon-enriched amorphous hydrogenated boron carbide films for very-low-k interlayer dielectrics. Adv Electr Mater 2017;3.
[3] Wang B, Shang YR, Ma Z, Pan L, Li YS. Non-porous ultra low dielectric constant materials based on novel silicon-containing cycloolefin copolymers with tunable performance. Polymer (Guildf) 2017;116:105–12.
[4] Cheng YL, Lee CY, Hung WJ, Chen GS, Fang JS. Comparison of various low dielectric constant materials. Thin Solid Films 2018;660:871–8.
[5] Okudur OO, Vanstreels K, Wolf ID, Hangen U, Qiu A. Substrate independent elastic modulus of thin low dielectric constant materials: substrate independent elastic modulus…. Adv Eng Mater 2017;19(8):1600653.
[6] Zizka J, King S, Every A, Sooryakumar R. Acoustic phonons and mechanical properties of ultra-thin porous low-k films: a surface brillouin scattering study. J Electron Mater 2018;47(7):3942–50.
[7] Yuan X, Wang Y, Zhu B. Adhesion between two carbon nanotubes: insights from molecular dynamics simulations and continuum mechanics. Int J Mech Sci 2018;138:323–36.
[8] Zha X, Jiang F, Xu X. Investigation of modelling and stress distribution of a coating/substrate system after an indentation test. Int J Mech Sci 2017;134:1–14.
[9] Okudur OO, Vanstreels K, Wolf ID, Hangen U. Extraction of elastic modulus of porous ultra-thin low-k films by two-dimensional finite-element simulations of nanoindentation. J Appl Phys 2016;119(2):8793–841.
[10] Ghidelli M, Sebastiani M, Collet C, Guillemet R. Determination of the elastic moduli and residual stresses of freestanding Au-TiW bilayer thin films by nanoindentation. Mater Des 2016;106:S0264127516307547.
[11] Deng G, Tieu A, Su L, Zhu H, Zhu Q, Zamri W, Kong C. Characterizing deformation behaviour of an oxidized high speed steel: effects of nanoindentation depth, friction and oxide scale porosity. Int J Mech Sci 2019;155:267–85.
[12] Xiang H, Li H, Tao F, Zhao Y, Cheng H, Gang Z, Peng X. Molecular dynamics simulation of AlN thin films under nanoindentation. Ceram Int 2016;43(5):138–45.
[13] Nawaz A, Mao WG, Lu C, Shen YG. Nano-scale elastic-plastic properties and indentation-induced deformation of amorphous silicon carbide thin film. Ceram Int 2017;43(1):385–91.
[14] Grashchenko AS, Kukushkin SA, Osipov AV, Redkov AV. Nanoindentation of GaN/SiC thin films on silicon substrate. J Phys Chem Solids 2017;102:151–6.
[15] Ozaki T, Koga T, Fujitsuka N, Makino H, Hohjo H, Kadoura H. Biaxial flexure testing of free-standing thin film membrane with nanoindentation system. Sensors Actuators A Phys 2018;278:48–59.
[16] Alauzet F, Fabrèges B, Fernández MA, Landajuela M. Nitsche-XFEM for the coupling of an incompressible fluid with immersed thin-walled structures. Comput Methods Appl Mech Eng 2016;301:300–35.
[17] Zhan Z, Hu W, Li B, Zhang Y, Meng Q, Guan Z. Continuum damage mechanics combined with the extended finite element method for the total life prediction of a metallic component. Int J Mech Sci 2017;124:48–58.
[18] Oliver WC, Pharr GM. An improved technique for determining hardness and elastic modulus using load and displacement sensing indentation experiments. J Mater Res 1992;7(6):1564–83.
[19] Bordas SPA, Rabczuk T, Hung NX, Nguyen VP, Natarajan S, Bog T, Quan DM, Hiep NV. Strain smoothing in FEM and XFEM. Comput Struct 2010;88(23–24):1419–43.
[20] Flemisch B, Fumagalli A, Scotti A. A Review of the XFEM-Based Approximation of Flow in Fractured Porous Media. In: Ventura G, Benvenuti E, editors. Advances in Discretization Methods. SEMA SIMAI Springer Series, vol. 12. Cham: Springer; 2016.
[21] Lehrenfeld C, Reusken A. Optimal preconditioners for Nitsche-XFEM discretizations of interface problems. Numerische Mathematik 2016;135(2):1–20.
[22] Kozlowski M, Kadela M, Gwozdz-Lason M. Numerical fracture analysis of foamed concrete beam using XFEM method. Appl Mech Mater 2016;837:183–6.
[23] Afshar A, Ardakani SH, Mohammadi S. Stable discontinuous space–time analysis of dynamic interface crack growth in orthotropic bi-materials using oscillatory crack tip enrichment functions. Int J Mech Sci 2018;140:557–80.
[24] Kired MR, Hachi BE, Hachi D, Haboussi M. Effects of nano-voids and nano-cracks on the elastic properties of a host medium: XFEM modeling with level-set function and free surface energy. Acta Mech Sinica 2019:1–13. doi:10.1007/s10409-019-00843-4.
[25] Meng Q, Wang Z. Extended finite element method for power-law creep crack growth. Eng Fract Mech 2014;127:148–60.
[26] Agathos K, Ventura G, Chatzi E, Bordas SPA. Stable 3D XFEM/vector-level sets for non-planar 3D crack propagation and comparison of enrichment schemes. Int J Numer Methods Eng 2018;113(2):252–76.
[27] Lee H, Vimonsatit V, Chindaprasirt P. Mechanical and micromechanical properties of alkali activated fly-ash cement based on nano-indentation. Construct Build Mater 2016;107:95–102.
[28] Chang SY, Tsai HC, Chang JY, Lin SJ, Chang YS. Analyses of interface adhesion between porous SiOCH low-k film and SiCN layers by nanoindentation and nanoscratch tests. Thin Solid Films 2008;84(16):319–27.
[29] Agathos K, Chatzi E, Bordas SPA, Talaslidis D. A well-conditioned and optimally convergent XFEM for 3D linear elastic fracture. Int J Numer Methods Eng 2016;105:643–77.
[30] Nian G, Shan Y, Qiang X, Qu S, Yang Q. Failure analysis of syntactic foams: a computational model with cohesive law and XFEM. Compos Part B Eng 2016;89:18–26.
[31] Takeda M, Matoba N, Matsuda K, Seki H, Inoue K, Oishi M, Sakai M. Effect of ultraviolet cure on the interfacial toughness and structure of SiOC thin film on Si substrate. J Mater Res 2010;25(10):1910–16.